Supplement of Geosci. Model Dev., 14, 3335–3359, 2021
https://doi.org/10.5194/gmd-14-3335-2021-supplement

Geoscientific Model Development
Open Access
EGU

Supplement of

Implementing a sectional scheme for early aerosol growth from new particle formation in the Norwegian Earth System Model v2: comparison to observations and climate impacts

Sara M. Blichner et al.

Correspondence to: Sara Marie Blichner (s.m.blichner@geo.uio.no)

Table 1. Sensitivity simulation overview. See detailed description in section 3.

Simulation	Description	Time step	Number of bins
$OAS_{bins=8}$	Increase number of bins	-	8
$OAS_{bins=3}$	Decrease number of bins	-	3
$OAS_{bins=8,0.1\times dt}$	Increase number of bins, reduce time step	3 minutes	8
$OAS_{0.1\times dt}$	Reduced time step	3 minutes	-
$OAS_{2\times dt}$	Not halved time step in condensation/nucleation.		-

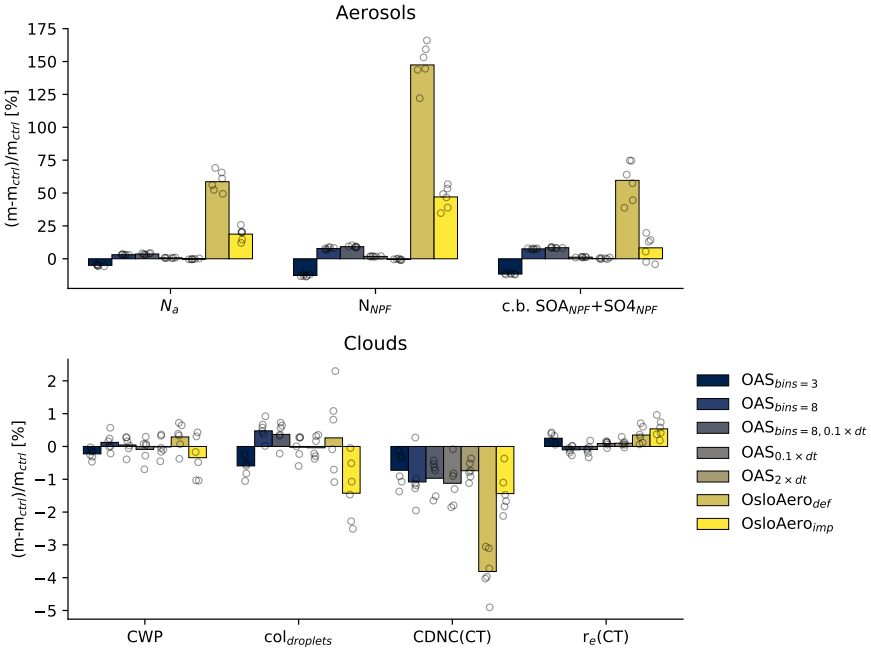

Figure S1. Globally averaged sensitivity runs over 2008–01 to and including 2008–06. Values of N_a and N_{NPF}, are near surface averages, that is pressure difference weighted averages up to 850 hPa.

1 Sensitivities

To investigate how sensitive the results are to the structure of the scheme , we performed several sensitivity tests where we varied the both the number of bins in the scheme and the timestep. As mentioned above, the quasi-stationary structure for the sectional scheme was chosen over e.g. the moving-center structure because it required fewer tracers and computational efficiency was a priority. However, it is known that the quasi-stationary structure is more prone to numerical diffusion than the moving-center structure.

These tests also indicate the strength of the numerical diffusion because it is known to decrease with increasing resolution of the bins. When varying the timestep, this has been done only for the nucleation, coagulation and condensation. These runs were performed for 1 year, where 6 months were discarded as spin up. They were all set up in the same way as the other runs in the paper, i.e. they have nudged meteorology, except that they are initialized from a run with the default model from 2007–01 to 2007–06. We show results from 2008–01 up to and including 2008–06. An overview of the sensitivity tests is shown in table 1.

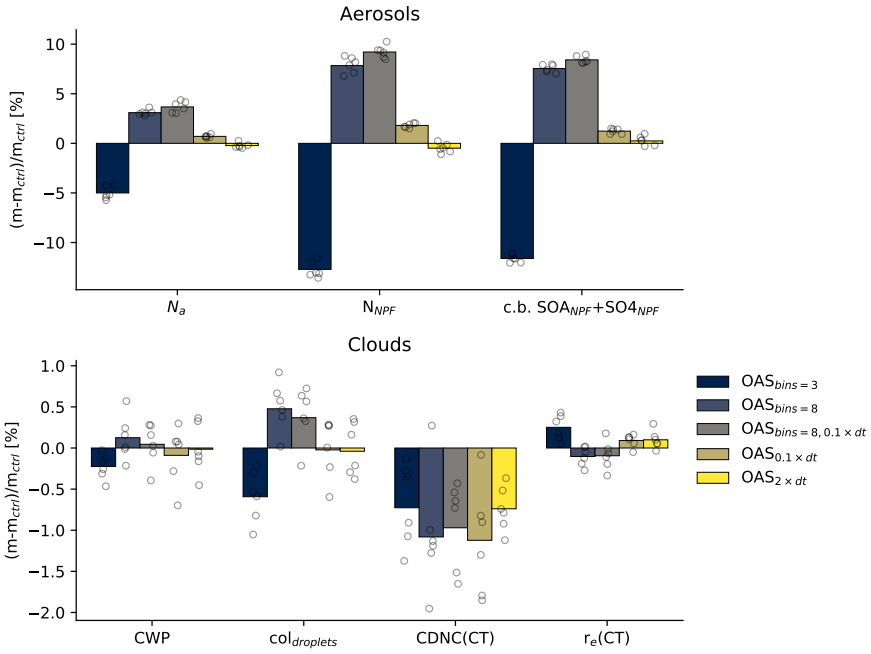

Figure S2. Globally averaged sensitivity runs over 2008–01 to and including 2008–06. Values of N_a and N_{NPF}, are near surface averages, that is pressure difference weighted averages up to 850 hPa.

Firstly we increase the number of bins from 5 to 8, $OAS_{bins=8}$, then we reduce the number of bins to 3, $OAS_{bins=3}$. Next, we reduce the time step by a factor of 0.1, thus to 3 minutes, $OAS_{0.1\times dt}$. Note that by default, the timestep is already halved for the condensation and nucleation code, so we also add a test for this, where the time step here is the same as for the rest of the model, $OAS_{2\times dt}$. Finally, we also test the combination of increasing the time step and the number of bins, $OAS_{bins=8,0.1\times dt}$.

Figures S1 and S2 show the relative difference between the sensitivity runs and a corresponding control run. Note that the difference between the figures is just that the first includes the default model for reference. The open circles show the monthly mean relative differences. The first row shows the aerosol properties, while the second shows cloud properties. In terms of aerosol differences, all the changes are below 5 % in terms of absolute aerosol number, N_a. However, the change in N_{NPF} and column burden of NPF particles (c.b. SOA_{NPF} +$SO4_{NPF}$), the change is as high as -12.7 % for reducing the number of bins ($OAS_{bins=3}$). On the other hand, increasing the number of bins to 8, gives a much smaller impact (∼7–8 %) and also increases the computational cost by 15 %. Changing the time step makes a modest impact ($OAS_{0.1\times dt}$ and $OAS_{2\times dt}$) results in a modest change NPF particles of below 2 %. Figure S3 shows the N_{NPF} concentrations globally averaged over latitude, longitude, and over the 6-month period of the simulation for the sensitivity runs. The default model runs for the same period are added for reference. These show that the changes between the sensitivity runs are homogeneous with height. On the other hand, the difference to the default model is larger near the surface, and reduced or even inversed with height.

In terms of impacts from cloud properties, the changes in the sensitivity runs are small (all below 2 %), and there is too much noise in these short runs to draw clear conclusions. However, the changes in cloud properties are likely smaller for the sensitivity tests than compared to the default model, especially cloud top cloud droplet number concentration (CDNC(CT)).

The changes are in general modest compared to the difference between the old and the new scheme (see Fig. S1). The changes due to time step are mostly minor, but the increase in particle number with increased number of bins (7–8 % for NPF particles) indicate that numerical diffusion does play some role. As always when developing ESMs, a balance must be struck between accuracy and keeping computational cost low.

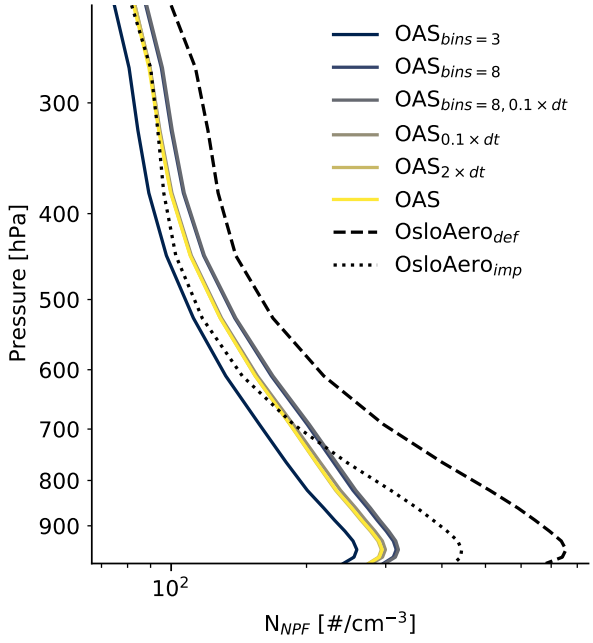

Figure S3. Globally averaged sensitivity runs over 2008–01 to and including 2008–06.

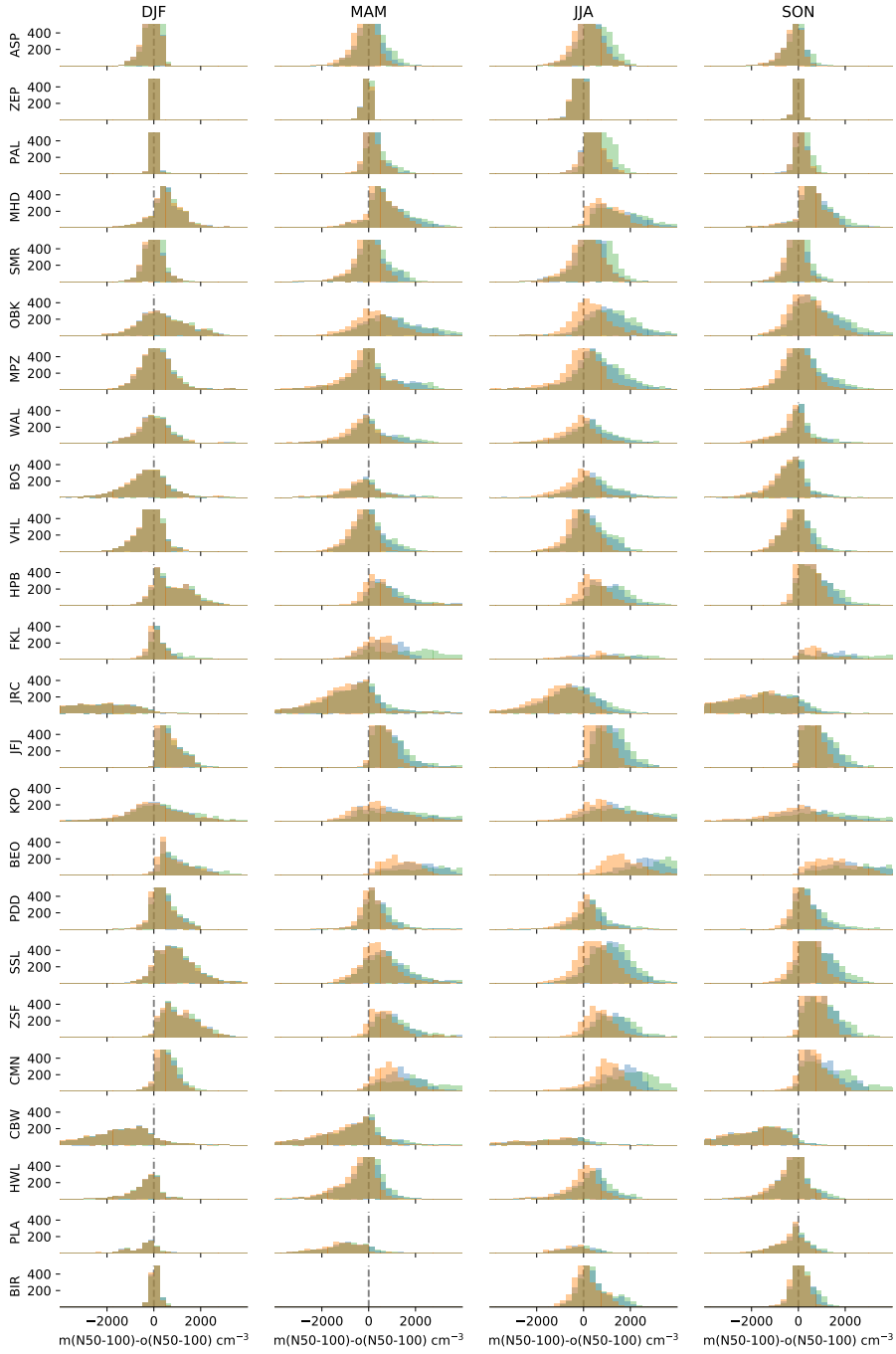

Figure S4. Histogram of modelled N_{50-100} minus observed N_{50-100} for each season and EUSAAR station (Asmi et al., 2011). We use hourly resolution and all available station data is is included. Zeppelin (ZEP), Mace Head (MHD), Aspvreten (ASP), SMEAR II (SMR), Pallas (PAL), Kosetice (OBK), Vavihill (VHL), Melpitz (MPZ), Waldhof (WAL), Bösel (BOS), Hohenpeissenberg (HPB), K-Puszta (KPO), JRC-Ispra (JRC), Finokalia (FKL), Jungfraujoch (JFJ), Schauinsland (SSL), Zugspitze (ZSF), Monte Cimone (CMN), BEO Moussala (BEO), Puy de Dôme (PDD) Preila (PLA), Birkenes b (BIR), Harwell (HWL), Cabauw (CBW).

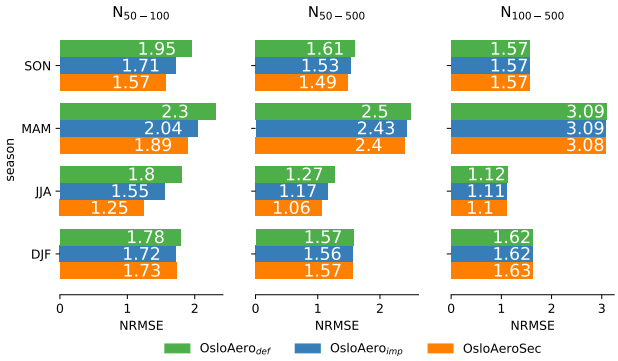

Figure S5. Normalized root mean square error (NRMSE) for each season and each model version compared to the EUSAAR dataset (Asmi et al., 2011). The root mean square error is normalized by the mean of the observed values.

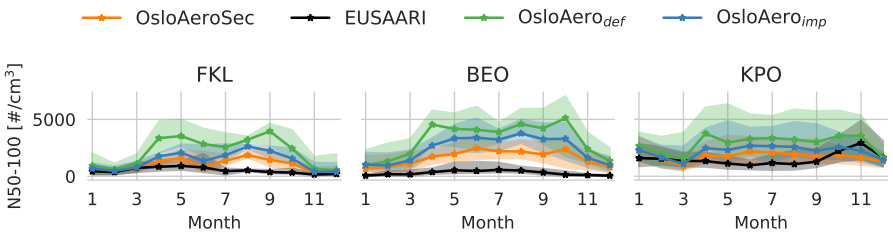

Figure S6. N_{50-100} monthly median (solid line) and percentiles (shaded, 16th to 84th) for stations with high concentrations. The plot is the same as 3, but displaying the full range of values which were cropped in figure 3.

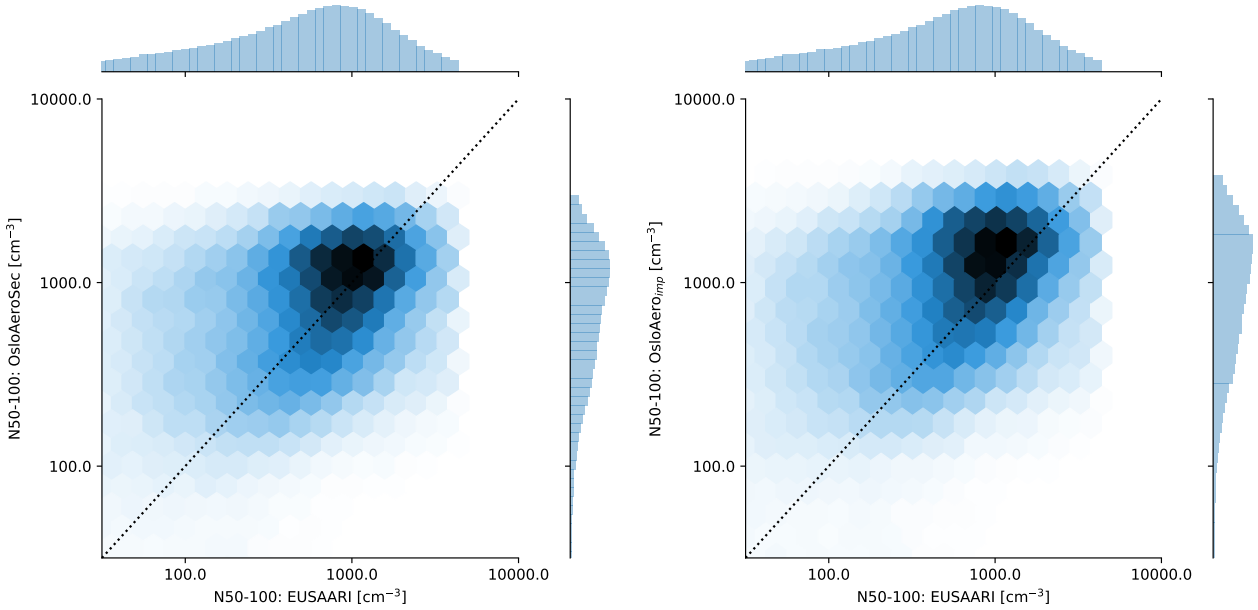

Figure S7. Two dimensional density distribution plots for N_{50-100} between modelled values (y-axis) and EUSAAR observations (x-axis). The left plot shows the relation for OsloAeroSec and the right for OsloAero$_{imp}$.

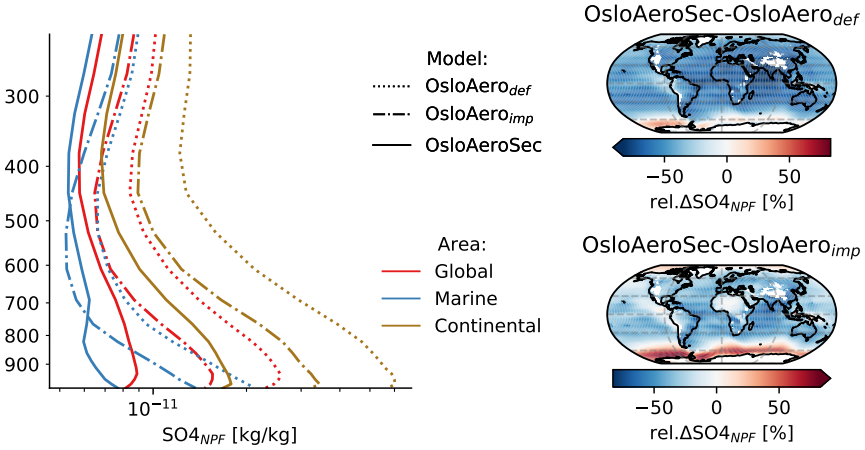

Figure S8. NPF particle mass in sectional scheme from H_2SO_4 ($SO4_{NPF}$). The plot to the left shows the average profiles over regions (global, marine and continental). The plots to the right show the near–surface average difference between OsloAeroSec and OsloAero$_{def}$ (top) and OsloAeroSec and OsloAero$_{imp}$ (bottom).

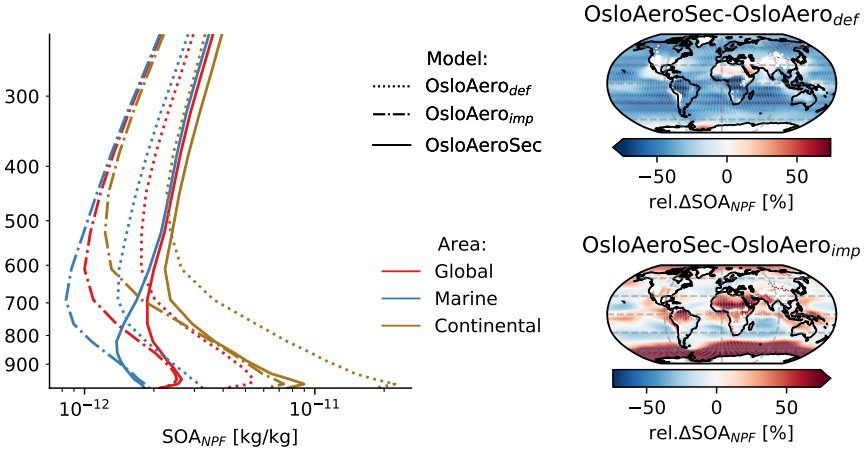

Figure S9. NPF particle mass in sectional scheme from SOAG$_{LV}$ (SOA$_{\text{NPF}}$). The plot to the left shows the average profiles over regions (global, marine and continental). The plots to the right show the near–surface average difference between OsloAeroSec and OsloAero$_{def}$ (top) and OsloAeroSec and OsloAero$_{imp}$ (bottom).

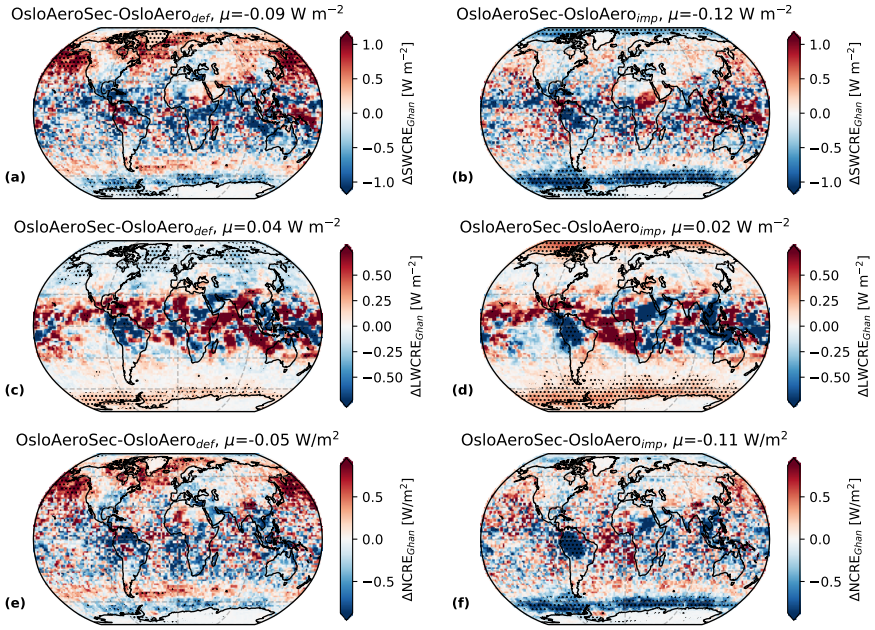

Figure S10. Difference in cloud radiative effect (CRE) for OsloAeroSec − OsloAero$_{def}$ (left) and OsloAeroSec − OsloAero$_{imp}$. Short wave CRE (SWCRE, top), long wave CRE (LWCRE, middle) and net CRE (NCRE, bottom)

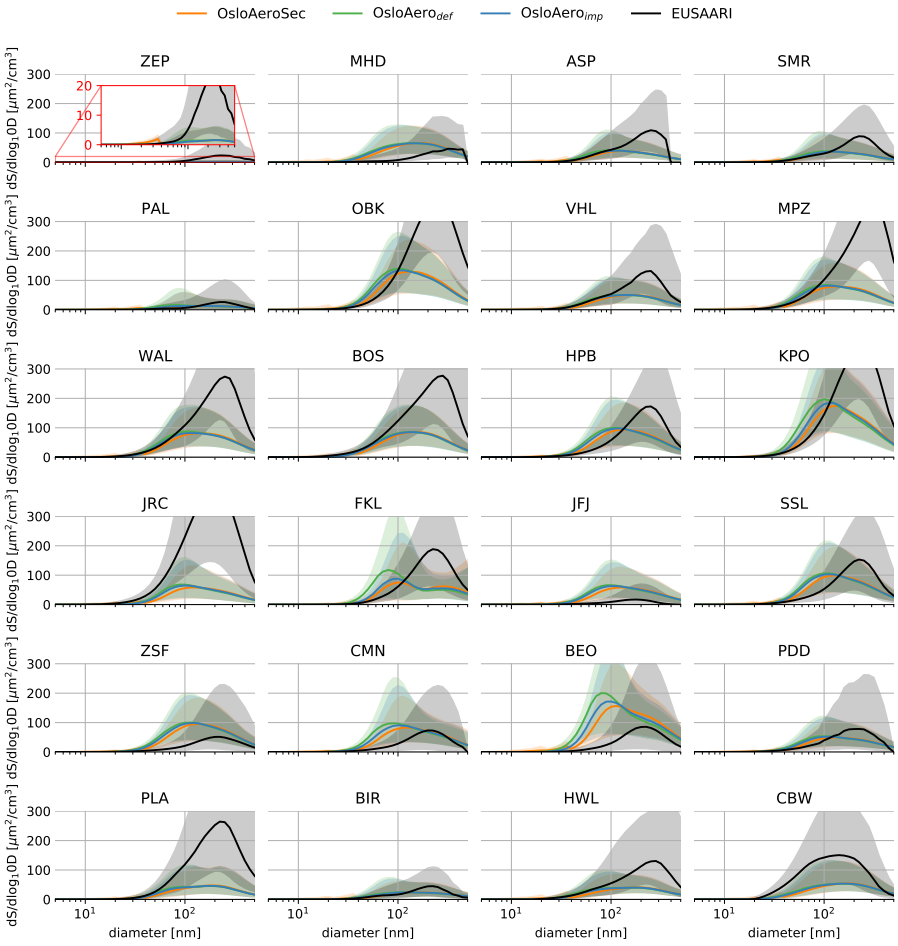

Figure S11. Median (solid line) particle surface size distribution and shading from 16th to 84th percentiles for observations and models. All data when and where observations are available is included.

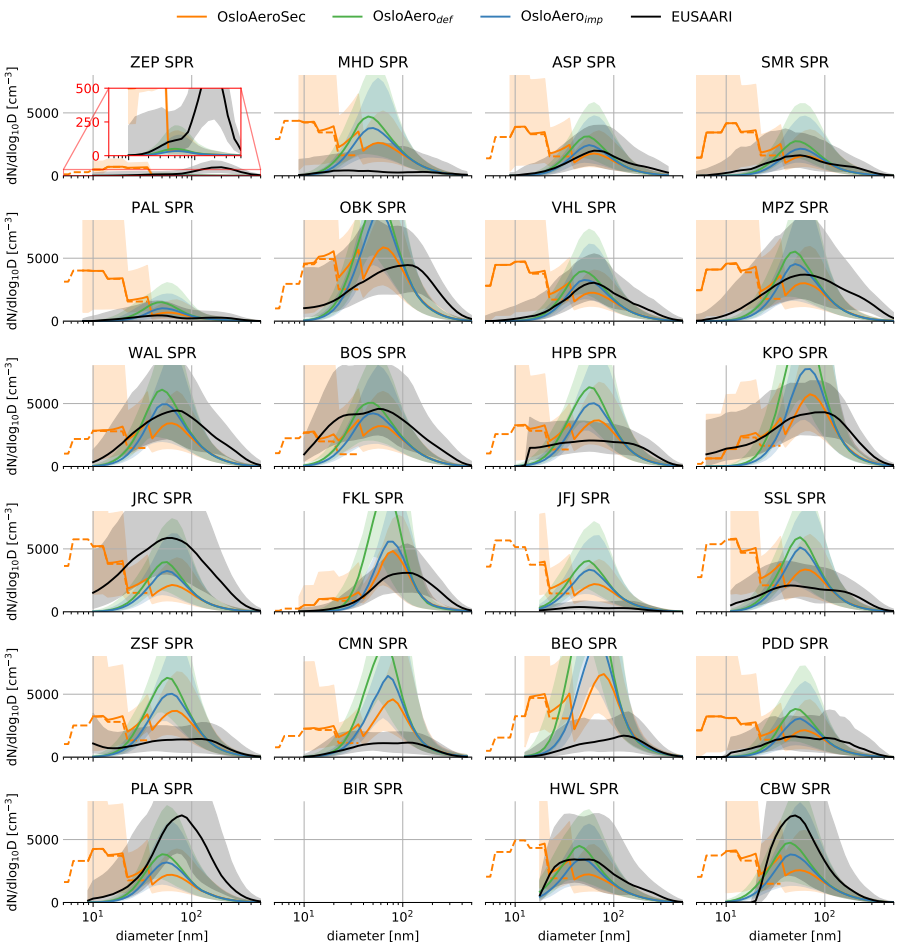

Figure S12. Spring: Median (solid line) and shading from 16th to 84th percentiles for observations and models for all valid datapoints.

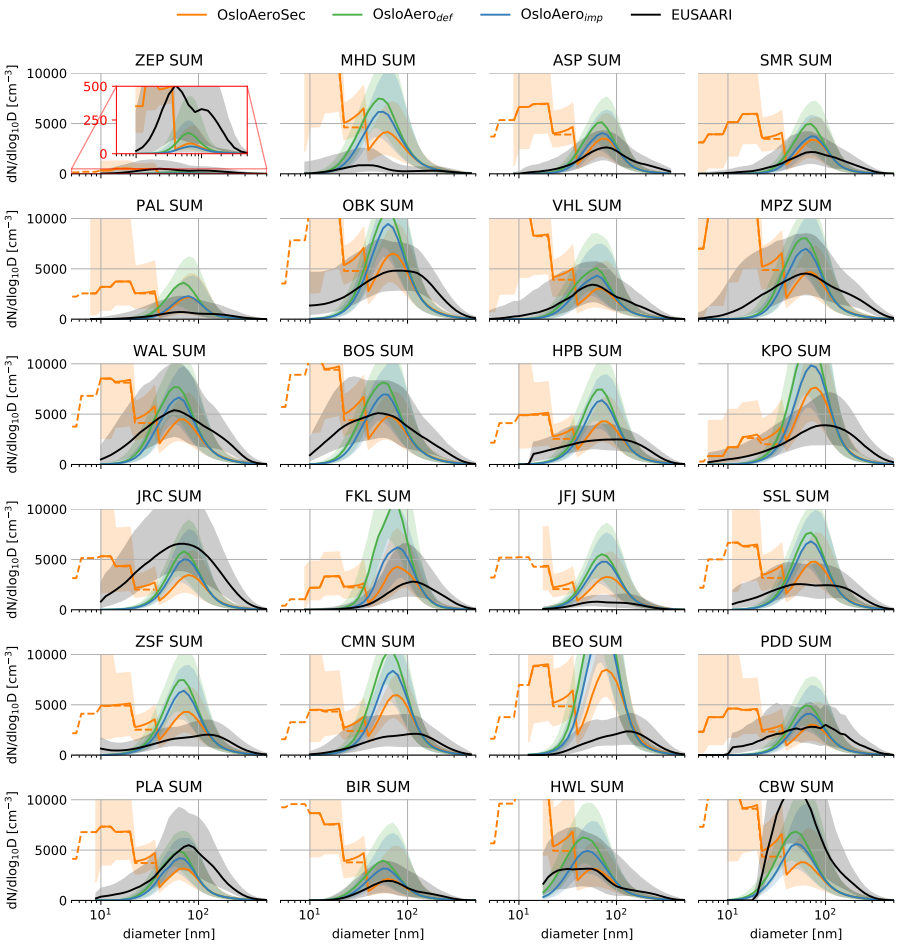

Figure S13. Summer: Median (solid line) and shading from 16th to 84th percentiles for observations and models for all valid datapoints.

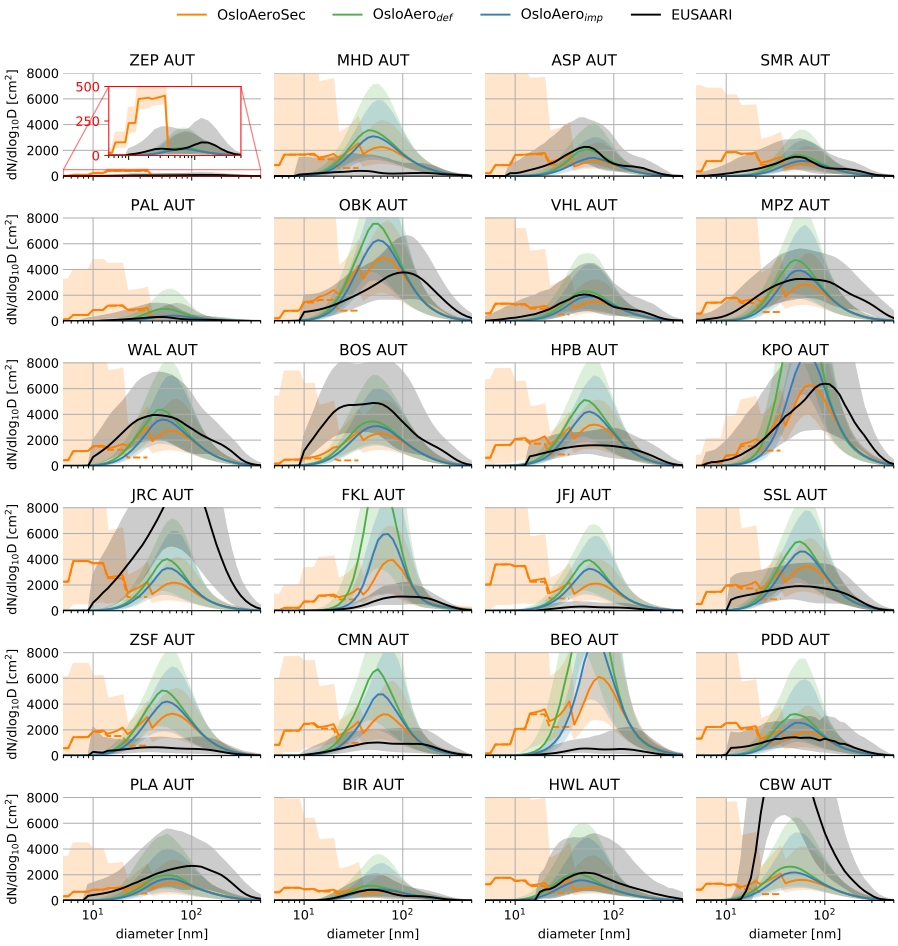

Figure S14. Autumn: Median (solid line) and shading from 16th to 84th percentiles for observations and models for all valid datapoints.

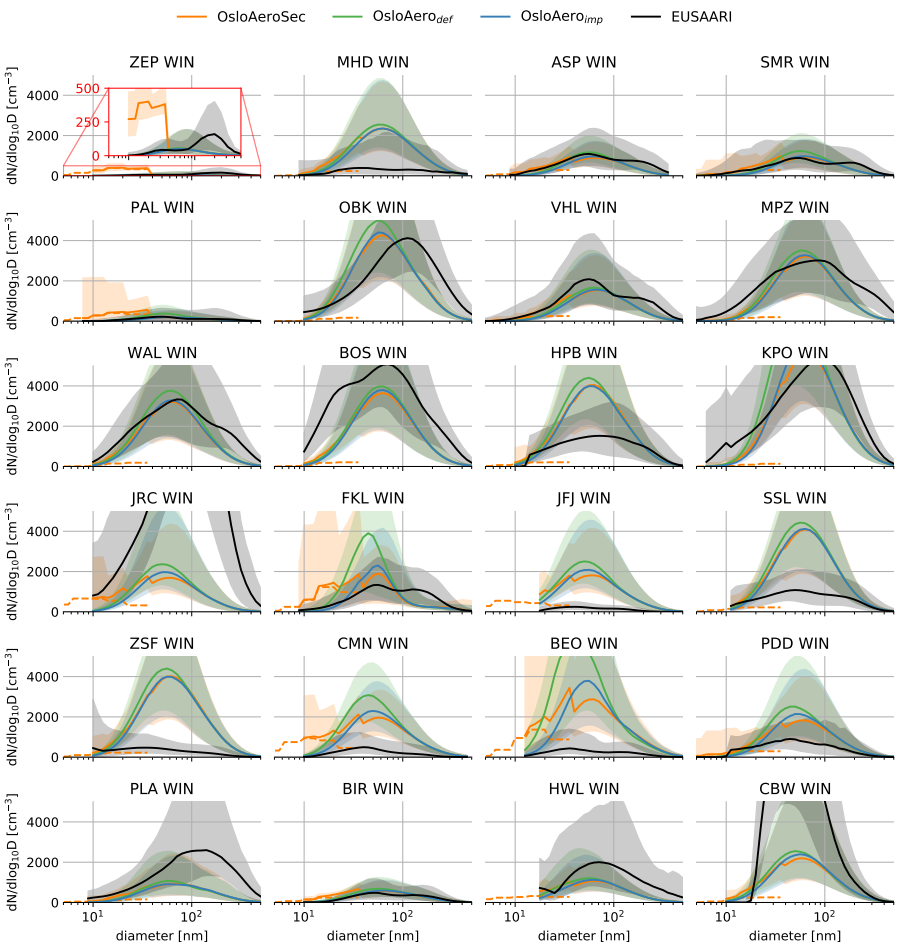

Figure S15. Winter: Median (solid line) and shading from 16th to 84th percentiles for observations and models for all valid datapoints.

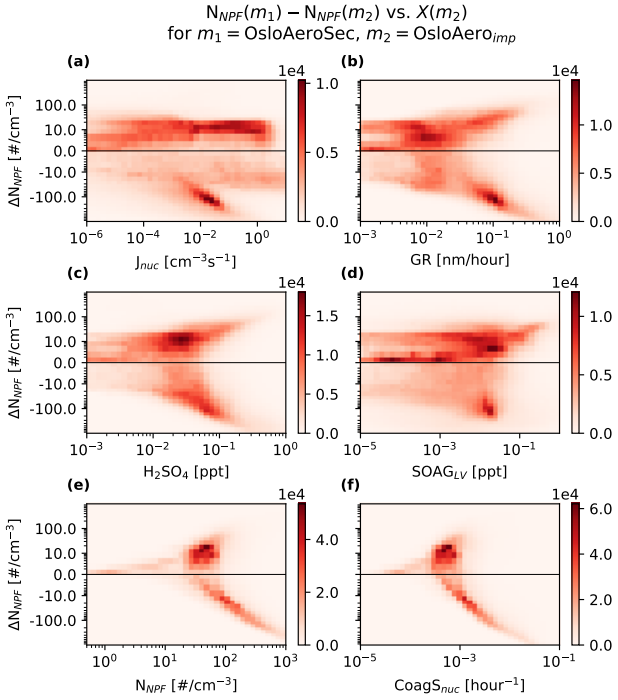

Figure S16. Same as 8, but comparing to OsloAero$_{def}$, rather than OsloAero$_{imp}$. Two-dimentional histogram of the relation between various factors in the original model run OsloAero$_{imp}$, and the change in number of particles from NPF, N_{NPF} between OsloAeroSec and OsloAero$_{def}$. The color shows the number of model grid cells which fall within the x,y-range using monthly mean files. Only grid cells below 100 hPa are included. The y-scale is linear between ± 5.

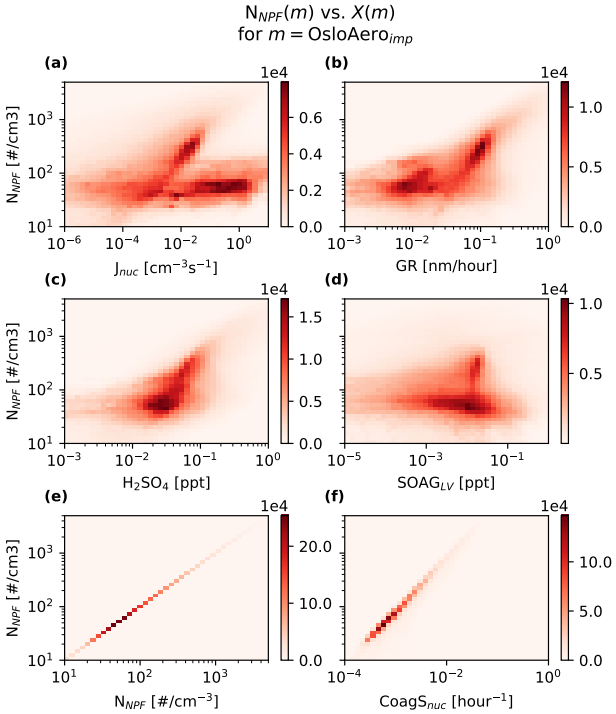

Figure S17. Two-dimensional histogram of the relation between N_{NPF} and various factors in the OsloAero$_{imp}$ simulation. 8, The color shows the number of model grid cells which fall within the x,y-range using monthly mean files. Only grid cells below 100 hPa are included.

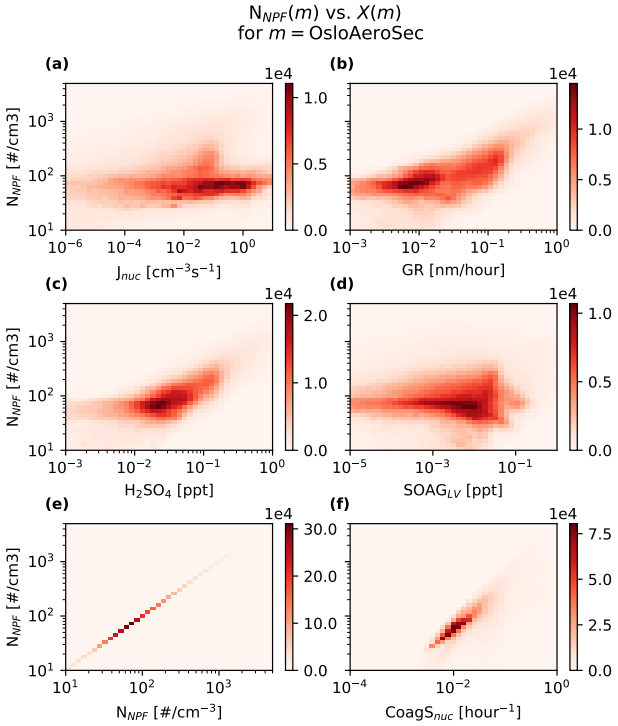

Figure S18. Two-dimensional histogram of the relation between N_{NPF} and various factors in the OsloAeroSec simulation. 8, The color shows the number of model grid cells which fall within the x,y-range using monthly mean files. Only grid cells below 100 hPa are included.

References

Asmi, A., Wiedensohler, A., Laj, P., Fjaeraa, A.-M., Sellegri, K., Birmili, W., Weingartner, E., Baltensperger, U., Zdimal, V., Zikova, N., Putaud, J.-P., Marinoni, A., Tunved, P., Hansson, H.-C., Fiebig, M., Kivekäs, N., Lihavainen, H., Asmi, E., Ulevicius, V., Aalto, P. P., Swietlicki, E., Kristensson, A., Mihalopoulos, N., Kalivitis, N., Kalapov, I., Kiss, G., de Leeuw, G., Henzing, B., Harrison, R. M., Beddows, D., O'Dowd, C., Jennings, S. G., Flentje, H., Weinhold, K., Meinhardt, F., Ries, L., and Kulmala, M.: Number Size Distributions and Seasonality of Submicron Particles in Europe 2008–2009, Atmospheric Chemistry and Physics, 11, 5505–5538, https://doi.org/10.5194/acp-11-5505-2011, 2011.